Journal of Catalysis 295 (2012) 186–194

Contents lists available at SciVerse ScienceDirect

Journal of Catalysis

journal homepage: www.elsevier.com/locate/jcat

CO_2-selective methanol steam reforming on In-doped Pd studied by in situ X-ray photoelectron spectroscopy

Christoph Rameshan [a,b], Harald Lorenz [a], Lukas Mayr [a], Simon Penner [a,*], Dmitry Zemlyanov [c], Rosa Arrigo [b], Michael Haevecker [b], Raoul Blume [b], Axel Knop-Gericke [b], Robert Schlögl [b], Bernhard Klötzer [a]

[a] Institute of Physical Chemistry, University of Innsbruck, Innrain 52a, A-6020 Innsbruck, Austria
[b] Department of Inorganic Chemistry, Fritz-Haber-Institute of the Max-Planck-Society, Faradayweg 4-6, D-14195 Berlin, Germany
[c] Purdue University, Birck Nanotechnology Center, 1205 West State Street, West Lafayette, IN 47907-2057, USA

ARTICLE INFO

Article history:
Received 31 May 2012
Revised 1 August 2012
Accepted 12 August 2012
Available online 11 September 2012

Keywords:
PdIn near-surface alloy
Pd foil
Methanol dehydrogenation
Methanol steam reforming
Water activation
In situ X-ray photoelectron spectroscopy (AP-XPS)

ABSTRACT

In situ X-ray photoelectron spectroscopy (in situ XPS) was used to study the structural and catalytic properties of Pd–In near-surface intermetallic phases in correlation with previously studied PdZn and PdGa.

Room temperature deposition of ~4 monolayer equivalents (MLEs) of In metal on Pd foil and subsequent annealing to 453 K in vacuum yields a ~1:1 Pd/In near-surface multilayer intermetallic phase. This Pd_1In_1 phase exhibits a similar "Cu-like" electronic structure and indium depth distribution as its methanol steam reforming (MSR)-selective multilayer Pd_1Zn_1 counterpart.

Catalytic characterization of the multilayer Pd_1In_1 phase in MSR yielded a CO_2-selectivity of almost 100% between 493 and 550 K. In contrast to previously studied In_2O_3-supported PdIn nanoparticles and pure In_2O_3, intermediate formaldehyde is only partially converted to CO_2 using this Pd_1In_1 phase. Strongly correlated with PdZn, on an In-diluted PdIn intermetallic phase with "Pd-like" electronic structure, prepared by thermal annealing at 623 K, methanol steam reforming is suppressed and enhanced CO formation via full methanol dehydrogenation is observed.

To achieve CO_2-TOF values on the isolated Pd_1In_1 intermetallic phase as high as on supported PdIn/In_2O_3, at least 593 K reaction temperature is required. A bimetal-oxide synergism, with both bimetallic and oxide synergistically contributing to the observed catalytic activity and selectivity, manifests itself by accelerated formaldehyde-to-CO_2 conversion at markedly lowered temperatures as compared to separate oxide and bimetal. Combination of suppression of full methanol dehydrogenation to CO on Pd_1In_1 inhibited inverse water–gas-shift reaction on In_2O_3 and fast water activation/conversion of formaldehyde is the key to the low-temperature activity and high CO_2-selectivity of the supported catalyst.

1. Introduction

Investigation of Pd–M (M = Zn, Ga, In) near-surface intermetallic phases (NSIPs) is critical for developing/improving Pd-based methanol steam reforming (MSR) catalysts. We aimed to extend our combined in situ X-ray photoelectron spectroscopy (in situ XPS) and kinetic studies on the palladium–zinc [1] and the Pd–Ga systems [2] to the catalytic activity/selectivity of an indium-doped Pd foil sample in MSR toward CO_2, formaldehyde, and CO. Similar to PdZn, palladium and indium form an 1:1 intermetallic compound exhibiting a density of states (DOSs) at the Fermi edge similar to that of Cu metal. Additional support for the electronic structure explanation of CO_2-selective methanol steam reforming via the Cu-like catalytic function of PdIn was expected.

Although both the "real" (i.e., small particles on oxide supports) and "inverse" (i.e., small oxide islands supported on metal foils or single crystals) model systems of PdZn have been scrutinized from both the structural and catalytic point of view and many aspects of the intermetallic formation and the structure–activity/selectivity interplay are already satisfactorily covered [1–19], the crucial details of the also highly selective supported Pd_xGa_y/Ga_2O_3 and Pd_x-In_y/In_2O_3 systems are less clear. There is common agreement that the presence of bimetallic phases of defined composition, formed after a reductive treatment at elevated temperatures, is beneficial for switching from CO-selective methanol dehydrogenation to CO_2-selective methanol steam reforming [3]. Recent investigations revealed the necessary presence of stable PdZn, Pd_2Ga, and PdIn bimetallic structures [3] and emphasized also the necessity of

* Corresponding author. Fax: +43 512 507 2925.
E-mail address: simon.penner@uibk.ac.at (S. Penner).

0021-9517
http://dx.doi.org/10.1016/j.jcat.2012.08.008

bimetallic bi-functional active sites for water activation and reaction of methanol to CO_2 [1,16]. Specifically for the "isolated" (i.e., unsupported) bimetallic Pd–Zn system, careful tuning of the intermetallic composition especially in surface-near regions turned out to be a prerequisite for the formation of these bifunctional active sites. In this respect, only a multilayer Pd–Zn surface alloy with a Pd/Zn = 1:1 composition exhibited a "Zn-up/Pd-down" corrugation affiliated with Pd_1Zn_1 surface entities being active for water splitting and exhibiting the formaldehyde-promoting "Cu-like" lowered density of states close to the Fermi edge [1,14]. The PdZn results already suggest to extend these PdZn inverse model studies to the corresponding intermetallic Pd–In inverse catalyst system, with the objective to extract the role of the single purely intermetallic PdIn surface regarding its specific catalytic properties without superimposed, potentially promoting metal-support interface effects. The related, highly CO_2-selective supported Pd_xIn_y/In_2O_3 catalyst [19] might indeed be strongly promoted by the "isolated" properties of the pure supporting oxide In_2O_3. Both supported catalyst and pure oxide have already been shown in recent contributions by some of the present authors, focusing both on the Pd–In_2O_3 interaction upon reduction of small In_2O_3-supported Pd particles in hydrogen [19] and the catalytic and reductive behavior of pure In_2O_3 [20–22]. In short, pure In_2O_3 is very susceptible to lose lattice oxygen upon annealing in hydrogen or CO [22] and is thus prone to strong metal-support interaction effects [19]. Most importantly, the reduced state of In_2O_3 is capable of activating water, but almost completely inactive in the reaction of CO_2 with oxygen defects to CO [22]. Hence, it does not catalyze the inverse water–gas shift reaction, which can spoil the CO_2-selectivity in methanol steam reforming. Moreover, pure In_2O_3 is, although being not very active, a rather selective methanol steam reforming catalyst with a CO_2 selectivity >95% at ~673 K reaction temperature [20]. This, however, sets In_2O_3 apart from ZnO [23,24] and Ga_2O_3 [25], which are both water–gas shift active and thus considerably less CO_2-selective, especially at elevated reaction temperatures.

Our primary aim therefore is to correlate the catalytic selectivity of In-metal and In_2O_3-modified Pd toward CO and CO_2 with in situ XPS and mass spectrometry under realistic MSR conditions. These studies are a further step toward the thorough understanding of the peculiar common catalytic properties of the pool of Pd-based intermetallic phases featuring CO_2-selective methanol steam reforming. The present studies again reveal the universal validity of the important concept of improved water activation by the dopant. In combination with the previously assumed electronic structure explanation for suppression of total dehydrogenation of methanol toward CO, and consequently enhanced formaldehyde formation, via the Cu-like electronic structure of PdIn [7,13–18], this provides a reliable basis for explanation of the pronounced CO_2-selectivity.

To correlate with the structure-insensitive total oxidation of methanol with O_2 toward CO_2 and water at low temperatures on the PdGa NSIP [2], two types of reforming reactions were studied in situ, namely "water-only" methanol steam reforming (MSR), corresponding to the "ideal" reaction $CH_3OH + H_2O \rightarrow CO_2 + 3H_2$, and oxidative steam reforming (OSR), whereby a certain added amount of O_2 may give rise to H_2-formation stoichiometries ranging from partial methanol oxidation ($CH_3OH + 1/2\ O_2 \rightarrow CO_2 + 2H_2$) to total oxidation ($CH_3OH + 3/2\ O_2 \rightarrow CO_2 + 2H_2O$). The interest in comparing MSR and OSR is basically derived from the fact that admission of a defined oxygen partial pressure to a methanol–water mixture is common to additionally suppress CO formation in the product stream by further CO oxidation and to compensate for the endothermicity of the pure methanol steam reforming reaction.

2. Experimental

2.1. Innsbruck experimental setup

The UHV system with attached all-glass high-pressure reaction cell [26] is designed for catalytic studies up to 1 bar on a larger piece of 1.8 cm × 2 cm polycrystalline Pd foil, allowing us to detect reaction products and even minor intermediates with high sensitivity, either by discontinuous sample injection into the gas chromatography–mass spectrometry (GC–MS) setup (HP G1800A) or by direct online MS analysis of the reaction mixture via a capillary leak into the GC/MS detector. The system consists of an UHV chamber with a long-travel Z-manipulator and a small-volume Pyrex glass reactor (52 ml, no hot metal components) attached to the outside of the UHV chamber and accessible via a sample transfer port. The UHV chamber is equipped with an XPS/Auger/ISS spectrometer (Thermo Electron Alpha 110) and a standard double Mg/Al anode X-ray gun (XR 50, SPECS), an electron beam heater, an ion sputter gun, and a mass spectrometer (Balzers).

For controlled In deposition, a home-built In evaporator was attached, which consists of a small boron nitride crucible filled with In metal (99.999%, Goodfellow) and heated by electron bombardment. A water-cooled quartz-crystal microbalance monitored the amount of deposited In.

The UHV-prepared samples are thereafter transferred by means of a magnetically coupled transfer rod from the UHV sample holder to a Pyrex glass sample holder used inside the all-glass reaction cell. With this all-glass setup of the ambient-pressure reaction cell, no wires or thermocouples are connected to the sample during catalytic measurement (thermocouple mechanically contacted at the outside). Accordingly, background (blind) activity of the reaction cell is routinely checked and no conversion was observed for all test reactions. A detailed graphic representation of the ambient-pressure reaction cell setup is provided in the Supplementary material (Fig. S1).

The main chamber is pumped by a turbomolecular pump, an ion getter pump, and a titanium sublimation pump to a base pressure in the low 10^{-10} mbar range. High-purity gases (H_2, O_2, Ar: 5.0) were used as supplied from Messer–Griesheim and dosed via UHV leak valves. The high-pressure cell is evacuated sequentially by a rotary pump (via LN_2 cooled zeolite trap) and then via the main chamber down to UHV base pressure and can be heated from outside to 723 K with an oven covering the cell. For better mixing of the reactants, the high-pressure cell is operated in circulating batch mode. By using an uncoated GC capillary attached to the high-pressure cell, the reaction mixture in the close vicinity of the sample is analyzed continuously by the electron ionization detector (EID) of the GC/MS system. For quantitative measurement of H_2, we used (in parallel to the EID) an additional Balzers QMA 125 detector specifically tuned for optimum H_2 detection. EID and QMS signals of methanol, CO_2, CO, H_2, and CH_2O were externally calibrated and corrected for fragmentation (i.e., CO and CH_2O fragments for methanol and CO fragment for CO_2).

A polycrystalline palladium foil (Goodfellow, purity 99.999%, 0.125 mm thick, size 3.5 cm^2) was cleaned on both sides by successive cycles of Ar^+ ion bombardment (6.0×10^{-5} mbar Ar, 503 eV, 1 μA sample current), oxidation (5.0×10^{-7} mbar O_2, T = 1000 K), and annealing in hydrogen (5.0×10^{-7} mbar H_2, T = 700 K) and in vacuum (T = 1000 K) until no impurities (surface carbon) were detected by AES and XPS. Details of the preparation of the PdIn multilayer intermetallic phase will be given in Section 3.1. Methanol and methanol/water mixtures were degassed by repeated freeze-and-thaw cycles. All MSR reactions were conducted with methanol/water mixtures of a 1:10 composition of the liquid phase. This corresponds to a room temperature partial pressure ratio of methanol/water = 1:2, as verified by mass spectrometry.

The catalytic experiments were performed in a temperature-programmed manner, that is, the reaction cell was heated at a constant linear rate of ~8 K/min to the final temperature of 623 K and then kept isothermal at this temperature for ~20 min. Experimental details will be given in context with the individual reaction runs. The advantage of the temperature programmed reaction (TPR) runs is that pronounced selectivity changes can be monitored via the partial pressure changes as a function of the reaction temperature, yielding useful qualitative information about changes of the reaction mechanism and the catalyst state. From the product partial pressures vs. time plots, the reaction rates were obtained by differentiation and are usually given in partial pressure change per minute (mbar/min), but whenever desired, the "idealized" turnover frequencies (TOF's) given in molecules per site and second ($site^{-1}\ s^{-1}$) can be calculated by multiplication of the partial pressure change with a factor $f = 4.8$, for example, a reaction rate of 1 mbar/min corresponds to a TOF of 4.8 $site^{-1}\ s^{-1}$. One "idealized active site" is viewed as a hypothetical Pd–In pair of surface atoms on the 1:1 intermetallic surface. Since this estimation yields the maximum conceivable number of active sites, the so-derived TOF values represent the lowest estimation limit. As a basis, we assumed a total number of potential catalytic surface sites $N_s = 5 \times 10^{15}$ on the entire 1:1 PdIn surface area of 7 cm^2 on the basis of equally distributed (1 1 1) and (1 0 0) facets. The conversion factor is based on the partial pressures of the reaction products already corrected for the temperature change in the reaction cell during the TPR run and for the steady removal of a fraction of the reaction mixture through the capillary leak. The correction has been achieved by adding 30 mbar Ar inert gas at the beginning of the reaction run and monitoring the $m/z = 40$ Ar intensity throughout the whole experiment. The Ar intensity over time then was used to recalculate the changes of the molar amounts of all products and reactants as referred to the initial state (before TPR start, reactor volume 60.6 ml and 300 K in the whole re-circulating batch system).

2.2. In situ XPS experimental setup

The in situ XPS system [27] at the beamline ISISS-PGM of BESSY II allowed us to perform in situ photoelectron spectroscopy up to 1 mbar total reactant pressures. It is equipped with differentially pumped electrostatic lenses and a SPECS hemispherical analyzer. The sample is positioned inside the near ambient-pressure chamber ~2 mm away from a 1 mm aperture, which is the entrance to the lens system separating gas molecules from photoelectrons. Binding energies (BEs) were generally referred to the Fermi edge recorded after each core level measurement. Samples were mounted on a transferable sapphire holder. The temperature was measured by a K-type Ni/NiCr thermocouple spot-welded to the side of the sample and temperature-programmed heating was done by an IR laser from the rear. Sample cleaning procedures consisted of repeated cycles of Ar^+ sputtering at room and elevated temperatures, annealing up to 950 K in UHV, and exposure to O_2, followed by flashing at 950 K for 60 s in UHV. The cleanliness of the Pd foil substrate was checked by XPS. The sensitivity of the simultaneous MS detection of the reaction products at NAP-XPS setup was not sufficient to extract reliable reaction rate and selectivity data for $H_2/CO/CH_2O/CO_2$, mainly because of an unfavorable ratio of the large total reactant flow through the XPS high-pressure cell (which is generally operated in constant flow mode) relative to the minor amounts of products formed on the low surface area catalyst (only ~0.5 cm^2 PdIn intermetallic surface on Pd foil). However, "connecting" experiments performed in the Innsbruck setup using the same conditions with respect to initial reactant pressures, PdIn NSIP preparation and reaction temperature range, allowed to assess a possible "pressure gap" effect and provided a reliable connection between the data obtained in either experimental setup.

Inelastic mean free paths (IMFPs) have been calculated on the basis of a formula given by Tanuma et al. for given photon energies [28]. We note, that for calculation, the element specific parameters of Ag have been used as an approximation, since the corresponding parameters of In are not known and Ag comes closest to the atomic mass of In.

3. Results and discussion

3.1. In deposition (4 MLE) followed by annealing from 323 K to 673 K in ultrahigh vacuum

Fig. 1 highlights the XPS spectra of the $Pd3d_{5/2}$, $In3d_{5/2}$, and valence band (VB) regions, taken after successive annealing steps in vacuum (5 min each) of a 4 MLE In film to various temperatures. The photon energies were adjusted to 570 eV (In3d), 460 eV (Pd3d), and 150 eV (VB) to ensure equal kinetic energies (and hence probe depths and equal electron scattering with the gas phase) for all three regions. A high degree of alloying was observed already at 300–350 K sample temperature, as evident from the room temperature spectra in Fig. 1. Between 300 K and 453 K, the Pd3d peaks gradually shifted from ~336.3 eV (below 373 K) to ~335.7 eV (Fig. 1) due to transition from an In-rich to a more In-depleted near-surface intermetallic phase. The related changes of the valence band spectra showed the expected transition from a "Cu-like" DOS (In-rich NSIP) to a "Pd-like" DOS (In-lean NSIP). Above 453 K, accelerated loss of near-surface indium into the Pd bulk occurred. The rather gradual change of the maximum position of the Pd3d signal from ~336.3 eV down to ~335.3 eV between RT and 673 K rather suggests a continuous transition from an In-rich to an In-depleted coordination chemistry of Pd (Fig. 2).

Analysis of depth profiling by photon energy variation (see Fig. 3, data derived from the XPS spectra shown in Fig. S2 of the supplementary material) showed both that the Indium concentration, at a given IMFP/kinetic energy, changes from In-rich to In-depleted conditions with increasing annealing temperature and that, at a given annealing temperature, an In concentration gradient persists. This gradient is strongest for the lowest annealing temperature (363 K: In/Pd = 63:37 at 0.4 nm to 51:49 at 1.0 nm IMFP). At high temperatures (623 K), the concentration gradient almost vanishes, and the In/Pd ratio remains around 19:81, irrespective of the XPS probe depth. According to the $In3d_{5/2}$ and $Pd3d_{5/2}$ peak areas obtained after annealing at 453 K, a ~48:52 = In/Pd composition is observed next to the surface (120 eV kinetic energy, inelastic mean free path of photoelectrons ~0.4 nm [29]. In deeper layers, the In/Pd ratio drops down to ~40:60 after 453 K-annealing (520 eV kinetic energy, ~1.0 nm IMFP). The 453 K annealing state thus exhibits the most similar electronic structure and Indium depth distribution as compared to the MSR-selective 1:1 PdZn "multilayer alloy" [1].

In summary, Figs. 1 and 2 show a continuous trend (with increasing annealing temperature) of the change of Pd electronic structure, due to the gradual lowering of coordination of Pd by In (gradual $Pd3d_{5/2}$ shift to lower BE). Vice versa, gradual increase in In coordination by Pd (equivalent to a gradual decrease in In coordination by In, $In3d_{5/2}$ shift to lower BE) is evident. Valence band related changes induced by changes in Pd–In coordination are accompanied by a strong shift of the Pd4d "center of mass" of density of states (DOSs) near the Fermi level to higher BE. VB spectra up to 453 K are "Cu-like", beyond 453 K they progressively change to "Pd-like". Considerable changes are induced beyond ~400 K, with a subsequent "transition region". Major changes, however, occur roughly between 423 K and 523 K.

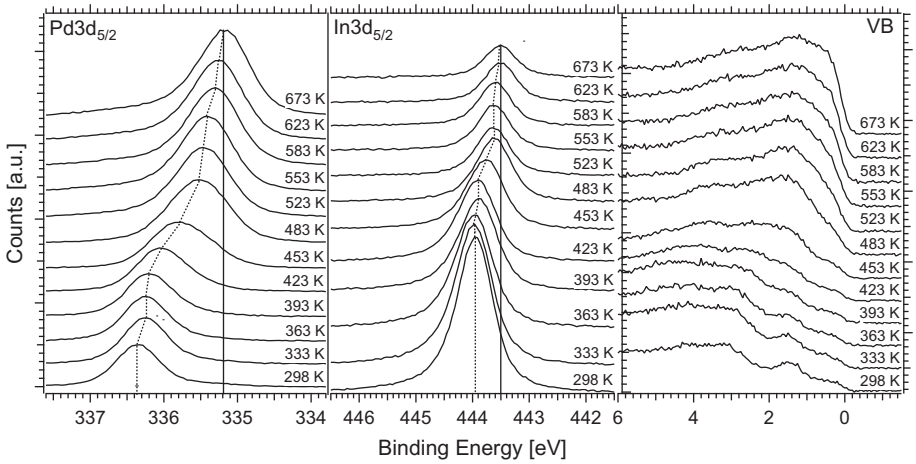

Fig. 1. XPS spectra of the $Pd3d_{5/2}$, $In3d_{5/2}$, and valence band (VB) regions, taken after successive anneals in vacuum (5 min each) of a 4 MLE In film to various temperatures. Photon energies were 570 eV (In3d), 460 eV (Pd3d), and 150 eV (VB) to ensure equal kinetic energies (probe depths) for all three regions. Spectra are unsmoothed data, normalized to the same photon flux. A Shirley background has been subtracted from the $Pd3d_{5/2}$ and $In3d_{5/2}$ signals.

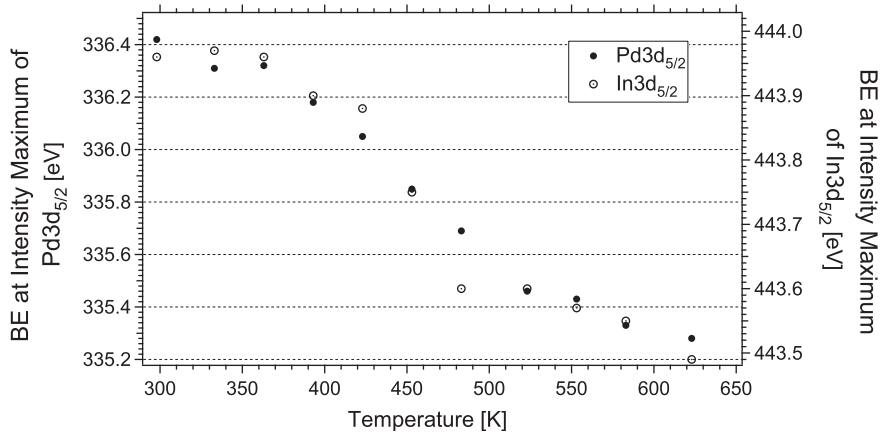

Fig. 2. Shift of the $Pd3d_{5/2}$ peak maximum position as a function of annealing temperature in vacuum.

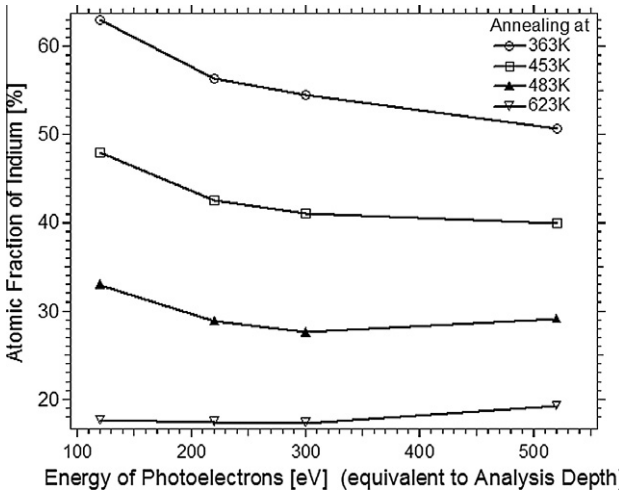

Fig. 3. Indium concentration profiles as a function of information depth after thermal annealing at 363 K, 453 K, 483 K, and 623 K, as derived from the data of Fig. S2. The energy of photoelectrons is equivalent to analysis depth and amounts to 0.45, 0.56, 0.66, and 0.92 nm.

Nevertheless, the stoichiometry changes with temperature are more gradual in nature as compared to the related PdZn NSIP, where a well-defined stability region of a 1:1 PdZn "multilayered" NSIP state was observed between ~500 K and ~570 K, but are in analogy to the PdGa NSIP [2], where more gradual changes of the near-surface composition with increasing annealing temperature have been observed, too.

Considering the Pd–In coordination in the surface-near regions, a simple charge transfer model yields a qualitative interpretation of relative BE shifts. With increasing temperature, the relative contribution of Pd–Pd coordination increases, as well as the Pd coordination of In. Considering a simple $Pd^{\delta+}$–$In^{\delta-}$ charge model, a relative decrease in the number of In–In (i.e., simultaneous increase in In–Pd) bonds should cause a relative increase in charge at the In centers and thus lowering of the In3d BE. In turn, a decreasing Pd3d BE is as well expected because Pd should be less positively charged in the "clean-Pd" state relative to the In-coordinated state. Analogous BE trends of Pd3d, Ga3d, and the VB region have already been observed on the related PdGa NSIP [2]. At this point, it must be emphasized that such a simple charge transfer model, based on (minor) electronegativity differences, cannot account for the strong covalent bonding character in the 1:1 intermetallic compounds such as Pd_1Ga_1 and Pd_1In_1, which will strongly

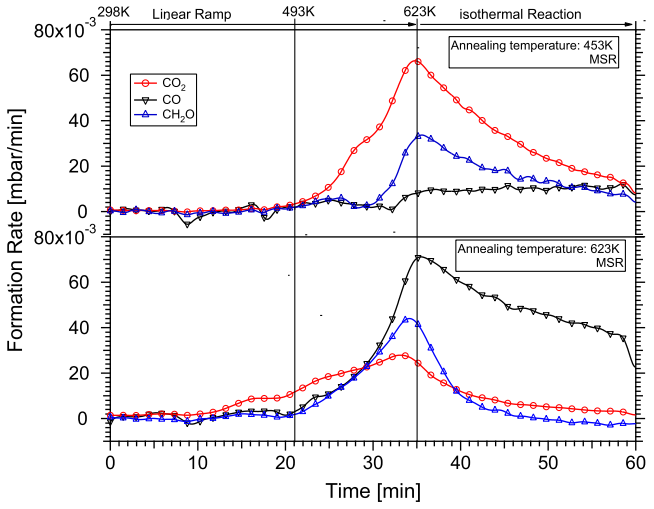

Fig. 4. Temperature-programmed methanol steam reforming on the "In-rich" 4 MLE PdIn NSIP annealed at 453 K (upper panel) vs. MSR reaction on "In-lean" PdIn NSIP (lower panel). Reaction conditions: 12 mbar methanol, 24 mbar water, 977 mbar He; linear temperature ramp (~8 K/min) up to 623 K, followed by isothermal reaction for 25 min. The decrease in the formation rates in the isothermal region is caused by progressive carbon-induced catalyst deactivation. Complete reaction mass balance involving stoichiometric hydrogen formation was verified by mass spectrometry analysis.

influence the electronic structure of the VB of the resulting solid phase. Nevertheless, neither the present Pd_1In_1 NSIP nor the related Pd_1Ga_1 NSIP has so far been shown to feature any structural analogies to the related bulk intermetallic phases (PdGa crystallizes in a cubic FeSi-structure, a = 0.489 nm, PdIn in cubic CsCl-structure, a = 0.326 nm). Rather, a "substitutional alloy" state with progressive replacement of Pd atoms by In (or Ga) within the basic Pd-fcc lattice represents an appropriate structure model [29]. Whether the relative mean charge on Pd and In is, because of this structural dissimilarity, markedly different for the bulk- and near-surface intermetallic phases, presently remains an open question.

Anticipating the catalytic experiments discussed in the subsequent sections, the model catalyst bimetallic initial state therefore is prepared by deposition of 4 MLE In followed by thermal annealing at 453 K. This appears reasonable because the data of Fig. 3 showed that the composition of surface layer and near-surface regions is closest to 1:1. It also shows an already improved thermal stability relative to lower annealing temperatures and comes closest to the PdZn~1:1 "multilayer" NSIP already studied in MSR [1], both with respect to the BE of Pd3d (~335.8 eV vs. ~335.9 eV) and the density of states at the Fermi edge ("Cu-like" electronic structure). A ~1:1 surface layer composition (with an already rather homogeneous depth distribution of In) is likely matched best. We, however, emphasize that the composition was solely extracted from XPS data. Unfortunately, low-energy ion scattering data for analysis of top layer composition are not available for PdIn, due to the too similar masses of Pd and In.

Hence, the ~48:52 = In/Pd NSIP present after annealing at 453 K was tested in the following as a model surface for methanol steam reforming ("MSR") and oxidative steam reforming ("OSR").

3.2. MSR reactivity studied in the recirculating batch reactor on the 4 MLE In NSIP annealed at 453 K and 623 K

The MSR measurements were performed in 12 mbar methanol + 24 mbar water and to simulate OSR conditions, 6 mbar O_2 were further added to this reaction mixture. Fig. 4 shows the results for the temperature-programmed methanol steam reforming reaction on the "In-rich" 4 MLE PdIn NSIP (annealed to 453 K, upper panel), and, for comparison, on an "In-lean" PdIn NSIP (annealed to 623 K, lower panel). For a better comparison to the respective experiments on the PdZn and PdGa NSIP's [1,2], the MSR reaction rates are given in mbar/min. To ensure an unambiguous correlation to the specific reaction (reactant/product partial pressure, temperature) conditions on other model systems and also supported systems, Figs. S3–S5 in the Supplementary material highlight the partial pressure changes of both the educts and MSR products during the reaction (mbar vs. reaction time) as well as the TOF data (in site^{-1} s^{-1}) vs. reaction time.

As it can be clearly seen, CO formation is almost completely suppressed on the 453 K-annealed PdIn-NSIP up to 623 K reaction temperature. A total conversion of 18% methanol was observed. CO_2 formation sets in at ~493 K and reaches its maximum rate at 623 K (6.6×10^{-3} mbar/min). Notable formation of formaldehyde (HCHO) is observed at ~550 K, reaching its maximum rate (3.4×10^{-3} mbar/min) also at 623 K. This indicates that the isolated PdIn-NSIP is already much more CO_2- than CO-selective, but complete conversion of the intermediate formaldehyde into CO_2 is not accomplished. At this stage, we want to emphasize that both the supported $PdIn/In_2O_3$ catalyst and the pure In_2O_3 support

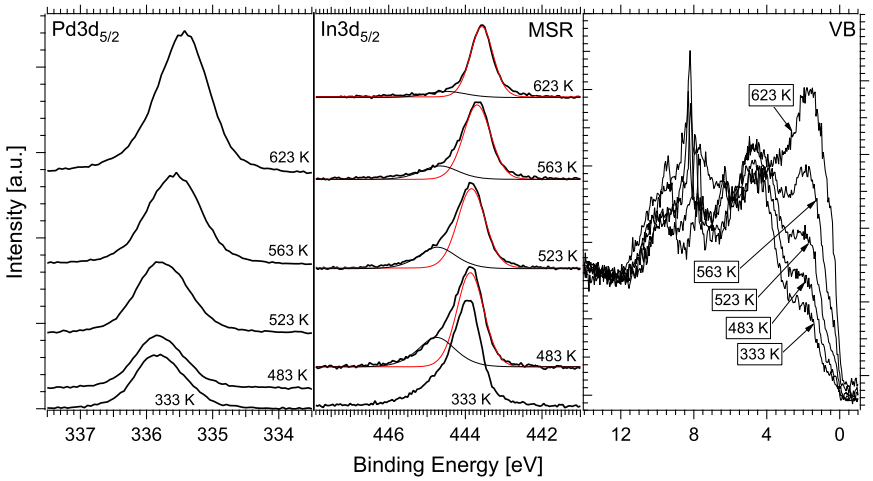

Fig. 5. $Pd3d_{5/2}$ core level spectra (left), $In3d_{5/2}$ spectra (middle) and VB spectra (right) obtained in situ during methanol steam reforming (0.07 mbar MeOH + 0.14 mbar H_2O) on the 4 MLE In NSIP annealed to 453 K in vacuum prior to reaction. $Pd3d_{5/2}$ and $In3d_{5/2}$ core level spectra were recorded with 460 eV and 570 eV photon energy, respectively, and the VB region with 150 eV in order to enhance the surface sensitivity.

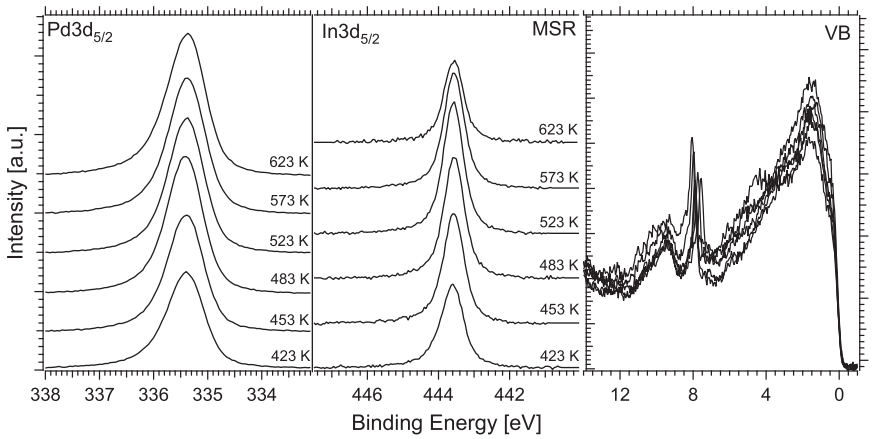

Fig. 6. $Pd3d_{5/2}$ core level spectra (left), $In3d_{5/2}$ spectra (middle), and VB spectra (right) obtained in situ during methanol steam reforming (0.07 mbar MeOH + 0.14 mbar H_2O) on the 1 MLE In NSIP. $Pd3d_{5/2}$ and $In3d_{5/2}$ core level spectra were recorded with 460 eV and 570 eV photon energy, respectively, and the VB region with 150 eV in order to enhance the surface sensitivity.

are highly CO_2-selective, but intermediary formed formaldehyde has never been detected [19,20]. This already indicates the importance of the bimetallic/support interface for quantitative oxidation of formaldehyde by water and is further corroborated by comparison of the measured TOF on the isolated PdIn-NSIP and on the In_2O_3-supported PdIn bimetallic. Iwasa and Takezawa [3] reports a TOF of 0.1 s^{-1} for CO_2 at 493 K (methanol/water 1:1 inlet partial pressures, 101 mbar each), the presented isolated model PdIn-NSIP annealed to 453 K exhibits a TOF of 0.007 s^{-1} at comparable temperatures. Only at ~590 K, a similar TOF value of ~0.1 s^{-1} is obtained. Arrhenius plots ln TOF vs. $1/T$ yield apparent activation energies of ~61 kJ/mole.

To simulate an In-leaner PdIn-NSIP, the 4 MLE PdIn-NSIP was additionally annealed to 623 K. As shown in the lower panel of Fig. 4, this results in a distinctly different selectivity pattern. As anticipated from previous experiments on PdZn, the selectivity pattern CO/CO_2 is now reversed and CO is the main product up to 623 K (~30 min reaction time). CO formation starts at around 493 K with an in parallel increase in formaldehyde. The formation rate of formaldehyde is higher than that of CO_2 at ~600 K (46×10^{-3} mbar/min compared to 26×10^{-3} mbar/min for CO_2). Note that according to Fig. 3, only ~20% In remains in the topmost surface layers, hence the surface-near regions are relatively Pd-rich, but a clear assignment to a surface "monolayer alloy" state similar to that of PdZn [1] (surface layer composition close to 1:1, but subsurface region strongly diluted) is not possible due to the inability to carry out reliable ion scattering experiments.

3.3. In situ XPS analysis during MSR on 1 MLE and 4 MLE In NSIP annealed at 453 K

Fig. 5 highlights the $Pd3d_{5/2}$ core level spectra (left), $In3d_{5/2}$ spectra (middle), and VB spectra (right) obtained in situ during methanol steam reforming (0.07 mbar MeOH + 0.14 mbar H_2O) on the 4 MLE In NSIP annealed to 453 K in vacuum prior to reaction. Both $Pd3d_{5/2}$ and $In3d_{5/2}$ core level spectra were recorded with 460 eV and 570 eV photon energy, respectively, and the VB region with 150 eV in order to enhance the surface sensitivity.

For the in situ spectroscopic analysis under more realistic MSR conditions, a 1:2 reaction mixture of 0.07 mbar methanol and 0.14 mbar water was used for all experiments, and the sample temperature was raised in 30 K steps from 298 to 623 K. Oxidized In appeared due to the influence of the MSR gas atmosphere, as evidenced by the shoulder of the $In3d_{5/2}$ peak at 444.7 eV in Fig. 5. However, in situ mass spectrometry detection at during in situ XPS experiment was not sensitive enough to detect the quite small reforming activity shown in Fig. 4 (which was only measurable with reasonable sensitivity in the batch reactor system at higher pressures). A shift of the thermally induced decomposition of the PdIn surface alloy was observed, that is, the initial bimetallic state of the catalyst was clearly stabilized by the gas phase and started to decompose only above 563 K under MSR conditions (for comparison see Figs. 1 and 2, showing a continuous change above 453 K).

Valence band spectra exhibit a Cu-like DOS at the Fermi edge up to about 523 K. The In $3d_{5/2}$ peaks do not show shifts up to 523 K, above which a "dilution" is observed and the In(ox) fraction is reduced, in close correlation to similar observations on the Pd_1Zn_1 monolayer NSIP [1]. At 623 K, only a very small amount of In(ox) is left, again in agreement with the Pd_1Zn_1 monolayer NSIP [1]. The respective 1 MLE In NSIP in situ analysis, shown in Fig. 6, yielded only a surface In/Pd ratio of ~24:76 (i.e., ~1:3).

The initial state (423 K) very much resembles the 623 K state in Fig. 5 (Pd3d at 335.4 eV, In3d at 443.6 eV), and this state does hardly change with increasing reaction temperature. Also the VB spectra are "Pd-like" right from the beginning and remain almost unchanged.

With respect to MSR performance, the selectivity pattern of this preparation resembled that of the 4 MLE/623 K sample (data not separately shown, cf. Fig. 4, lower panel). Nevertheless, it still showed the expected *relative* selectivity trends in comparison to clean, undoped Pd foil both in the QMS analysis and the batch reactor experiments, namely a relative promotion of formaldehyde and CO_2 formation as well as suppression of CO formation relative to clean Pd foil. Not too surprisingly, the total CO_2-selectivity was not as good as in the 4 MLE/453 K case (compare Fig. 4, upper panel) and almost no oxidized In was observed during reaction.

3.4. OSR reactivity studied in the recirculating batch reactor setup on4 MLE In-doped Pd-foil annealed at 453 K

Temperature-programmed oxidative steam reforming reactions (OSR) have additionally been carried out (Fig. 7). Experimental conditions were similar to those of the methanol steam reforming reaction with the one exception of 6 mbar O_2 additionally admitted to the steam reforming mixture (OSR reactant mixture: 12 mbar methanol, 24 mbar water, 6 mbar O_2). Measurements have been carried out on the "In-rich" 4 MLE PdIn NSIP prepared at 453 K (lower panel) in comparison with the MSR reference reaction (i.e., without O_2) on the same initial NSIP state (upper panel). As

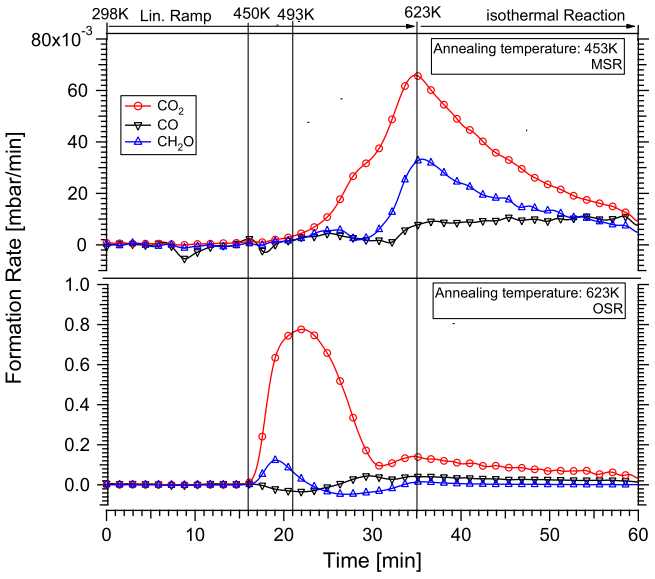

Fig. 7. Temperature-programmed OSR (initial reactant mixture: 12 mbar methanol, 24 mbar water, 6 mbar O_2) on the "In-rich" 4 MLE PdIn NSIP annealed at 453 K (lower panel) vs. MSR reference reaction (without O_2) on the same initial NSIP state (upper panel); linear temperature ramp (~8 K/min) up to 623 K, followed by isothermal reaction for 25 min.

revealed by Fig. 7, in striking contrast to the pure MSR reaction, the OSR reaction sets in a much lower temperature, that is, at around 450 K. CO_2 is the primary oxidation product up to ~580 K, at which temperature full consumption of the initially added 6 mbar O_2 is attained. The maximum CO_2 formation rate is about 0.8 mbar/min (3.84 site^{-1} s^{-1}) at 493 K, which is considerably higher than under simple MSR conditions at 623 K.

Comparing MSR and OSR, the selectivity trends in terms of CO_2, CO, H_2, and H_2O formation were quite similar to those observed on the "multilayered" PdGa-NSIP. Under MSR conditions, CO_2 formation was found to be dominating up to 623 K reaction temperatures with almost entirely suppressed CO formation. Under OSR conditions, accelerated CO_2 formation was observed at lower temperatures (~423 K) [compare Fig. 8 in Ref. 2].

The time-resolved H_2-mass balance of the OSR reaction run of Fig. 7 has been deduced from the relative consumption of methanol by reaction with O_2 toward CO_2 (T < 580 K) and by dehydrogenation toward CO (>580 K) and is also represented graphically in the Supplementary material (Fig. S6–8). During the oxygen-consuming reaction, about 31% of the converted methanol is totally oxidized to CO_2 and water, and a ~69% contribution of partial oxidation toward CO_2 and H_2 is observed. In conclusion, only this minor fraction of the methanol becomes partially oxidized, according to the reaction stoichiometry $CH_3OH + 1/2\ O_2 \rightarrow CO_2 + 2H_2$. Nevertheless, this proves that a reaction pathway for a hydrogen-producing reaction even in the simultaneous presence of O_2 is possible and that total oxidation according to the stoichiometry $CH_3OH + 3/2\ O_2 \rightarrow CO_2 + 2H_2O$ does not take place exclusively. Moreover, the very high CO_2-selectivity in the temperature range around 500 K indicates that O_2-addition could indeed be helpful to optimize CO_2 selectivity and to efficiently suppress the CO content of the reformate gas also under continuous flow reaction conditions.

In summary, a highly CO_2 selective, combined total/partial oxidation reaction was obtained under OSR conditions in the temperature region ~450–580 K. The 4 MLE In/453 K annealed NSIP is capable of efficiently activating oxygen at low temperatures, while being mostly inactive for CO formation at the same time. Methanol is converted by O_2 to CO_2 via combined total/partial oxidation of intermediary formed C_1-oxygenates at the surface with some simultaneous hydrogen production. Since we are not aware of methanol total or partial oxidation TOF's measured on any of the literature-reported PdGa or PdZn systems, a comparison of the OSR rates between model and real systems is currently not possible. Above ~580 K (i.e., after quantitative O_2 consumption), water-driven yet CO_2 selective MSR is observed. The CO- and CO_2-selectivities at 623 K are around 14% and 86%, respectively, and the maximum CO_2 activity at 623 K (gas-phase composition 8 mbar CO_2 and 0.2 mbar CO) amounts up to 0.12 mbar/min (0.29 site^{-1} s^{-1}), which is comparable to the maximum value of 0.068 mbar/min (0.16 site^{-1} s^{-1}) for "simple" MSR at 623 K (Fig. 7 upper panel), especially when accounting for the already lowered methanol reactant pressure. The latter result also implies that the PdIn NSIP is rather stable in the presence of O_2, because strong, irreversible oxidative decomposition of the NSIP toward Pd and In_2O_3 while being exposed to the O_2 partial pressure would be eventually accompanied by a strong selectivity shift toward CO at T > 580 K, which was not observed. This relatively high segregation stability will be described from the following AP-XPS section.

3.5. In situ XPS analysis during OSR on the 4 MLE In-doped Pd-foil annealed at 453 K

For the in situ spectroscopic analysis under more realistic OSR conditions, a 1:2:0.5 reaction mixture of 0.07 mbar methanol,

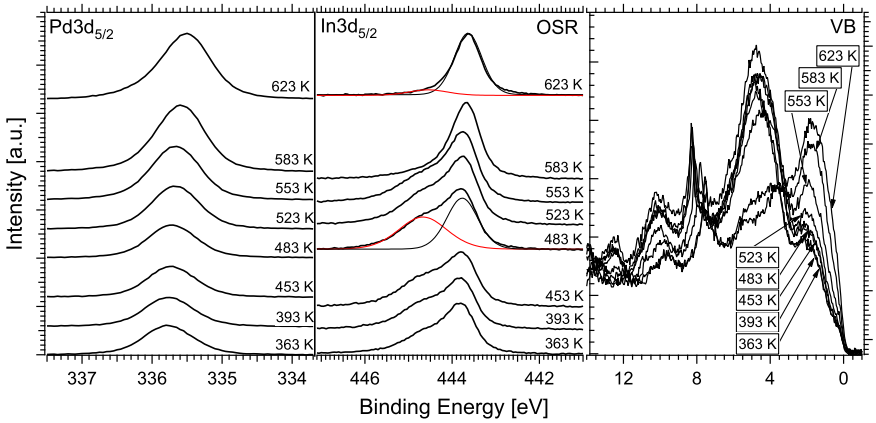

Fig. 8. $Pd3d_{5/2}$ core level spectra (left), $In3d_{5/2}$ spectra (middle), and VB spectra (right) obtained in situ during oxidative methanol steam reforming (0.07 mbar MeOH + 0.14 mbar H_2O + 0.035 mbar O_2) on the 4MLE In NSIP annealed to 453 K in vacuum prior to reaction. $Pd3d_{5/2}$ and $In3d_{5/2}$ core level spectra were recorded with 460 eV and 570 eV photon energy, respectively, and the VB region with 150 eV in order to enhance the surface sensitivity.

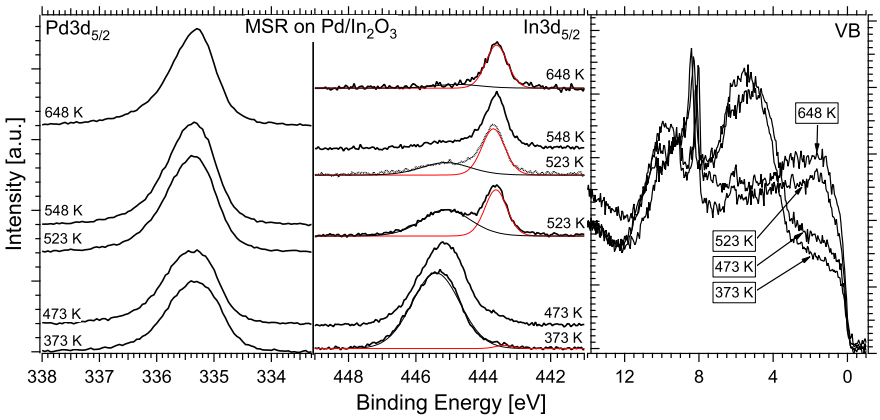

Fig. 9. $Pd3d_{5/2}$, $In3d_{5/2}$, and VB regions on the initial In_2O_3-on-Pd "inverse catalyst" showing the transition from the initial oxide-on-metal state to the intermetallic InPd state in the temperature region around 523 K under MSR conditions.

0.14 mbar water and 0.035 mbar O_2 was used, and the sample temperature was again raised in 30 K steps from 363 to 623 K. In comparison to MSR without added O_2, an increased amount of oxidized indium (In3d component at 444.7 eV in Fig. 8, relative to MSR induced In(ox) at 444.7 eV in Fig. 5), was observed in situ under OSR conditions between 363 and 553 K, along with strongly diminished carbon contamination.

Despite the more oxidizing conditions, the bimetallic near-surface catalyst state turned out to be stable up to ~553 K (Pd3d position remaining around 335.8 eV).

At 583 K, already a slight shift toward a lower BE of Pd3d (~335.6 eV) is visible, probably due to progressing dilution of In into deeper layers by bulk diffusion, but at 623 K the Pd3d BE of 335.5 eV is still markedly above the value of clean Pd (335.0 eV). Surprisingly, at 583 K, the 444.7 eV In(ox) component has disappeared rather than increased, which means that In(ox) becomes fully reduced to the bimetallic PdIn state even in the presence of O_2. This reduction is necessarily caused by the ongoing methanol oxidation, which obviously consumes In(ox) at increasing rates with increasing reaction temperature. Due to the pronounced thermal and chemical stability of the PdIn NSIP, both in the high-pressure MSR and OSR experiments, hardly any selectivity shift toward CO due to the thermally and/or oxidatively induced decay of the NSIP was observed (see also Fig. 7, lower panel). This result is in strong contrast to our observations both on the related PdZn and PdGa NSIPs, where a clear selectivity shift toward CO was observed at temperatures above 573 K [1,2].

3.6. In situ XPS analysis under MSR conditions starting from In_2O_3-covered Pd metal

This "inverse" In_2O_3/Pd-metal catalyst was prepared by reactive deposition of 1 MLE In in a background of 10^{-5} mbar of oxygen, followed by post-oxidation in 0.1 mbar oxygen at 453 K. Thereafter, MSR was started on the In_2O_3 covered surface on an otherwise electronically unaltered Pd substrate (initial BE of $Pd3d_{5/2}$ at 335.1 eV). Up to ~523 K, indium remained mostly in the oxidized state, and the presence of monometallic Pd gave rise to predominant CO formation. At 523 K, indium is gradually reduced, as shown in Fig. 9, and the surface "switches" to a diluted bimetallic state, as documented by both the In3d and VB spectral changes. Pd3d remains in the region below 335.5 eV, because the reduction temperature is already too high to allow for a multilayer NSIP state. These results prove that the PdIn-NSIP is also the thermodynamically stable phase under MSR conditions.

4. Conclusions

With respect to mechanism, the hypothesis that "In-poisoning" of Pd shifts the selectivity in methanol steam reforming toward formaldehyde, and subsequently also CO_2 is selectively formed from formaldehyde (as a consequence of improved water activation), is again verified in our PdIn "inverse" model study. With respect to differences to the related supported catalysts and pure In_2O_3, there are strong indications for a bimetal–oxide bi-functional synergism on the supported catalysts. Similar to the PdZn/ZnO and Pd_2Ga/Ga_2O_3 cases, the interplay between oxidic support and bimetallic surface induces three desirable catalytic effects:

(1) Lowering of onset temperature of reforming relative to both the clean oxide and the isolated, unsupported PdIn NSIP.
(2) Enhanced selectivity toward CO_2, as compared to both isolated oxide and PdIn NSIP.
(3) Enhanced reforming rate to CO_2 at comparably lower temperatures.

Altogether, the "bifunctional synergism" between oxide and bimetal can be pinned down to the three advantages mentioned above for all three systems. It appears likely that the active area of the bimetal–oxide interface is particularly suited to lower the individual activation barriers of the required sequence of elementary reaction steps by conducting the respective process at the place where they work most efficiently. Most likely, water activation is improved at reduced (defective) oxidic (interface) centers, whereas hydrogen and CO_2 desorption likely is less activated on the bimetallic surface, which can promote CO_2-selective formate decarboxylation and suppress unwanted decarbonylation processes.

Acknowledgments

This work was financially supported by the Austrian Science Fund (FWF) through grants P20892-N19 and F4503-N16. Ch. Rameshan acknowledges a PhD scholarship granted by the Max Planck Society. Support for the measurements at HZB/BESSYII was granted through EU program RII-3-CT-2004-506008, proposal no. 2011_1_101360. The authors thank the BESSY staff for their support of the in situ XPS measurements.

Appendix A. Supplementary material

Supplementary data associated with this article can be found, in the online version, at http://dx.doi.org/10.1016/j.jcat.2012.08.008.

References

[1] Ch. Rameshan, W. Stadlmayr, C. Weilach, S. Penner, H. Lorenz, M. Hävecker, R. Blume, T. Rocha, D. Teschner, A. Knop-Gericke, R. Schlögl, N. Memmel, D. Zemlyanov, G. Rupprechter, B. Klötzer, J. Catal. 276 (2010) 101;
Ch. Rameshan, W. Stadlmayr, C. Weilach, S. Penner, H. Lorenz, M. Hävecker, R. Blume, T. Rocha, D. Teschner, A. Knop-Gericke, R. Schlögl, N. Memmel, D. Zemlyanov, G. Rupprechter, B. Klötzer, Angew. Chem. Int. Ed. 49 (2010) 3224.

[2] Ch. Rameshan, W. Stadlmayr, S. Penner, H. Lorenz, M. Hävecker, R. Blume, T. Rocha, D. Teschner, A. Knop-Gericke, R. Schlögl, N. Memmel, D. Zemlyanov, B. Klötzer, J. Catal. 290 (2012) 126–137.

[3] N. Iwasa, N. Takezawa, Top. Catal. 22 (2006) 215.

[4] S. Penner, B. Jenewein, H. Gabasch, B. Klötzer, D. Wang, A. Knop-Gericke, R. Schlögl, K. Hayek, J. Catal. 241 (2006) 14.

[5] J.D. Holladay, Y. Wang, E. Jones, Chem. Rev. 104 (2004) 4767.

[6] M. Lenarda, E. Moretti, L. Storaro, P. Patrono, F. Pinzari, E. Rodriguez-Castellon, A. Jimenez-Lopez, G. Busca, E. Finocchio, T. Montanari, R. Frattini, Appl. Catal. A 312 (2006) 220.

[7] A. Bayer, K. Flechtner, R. Denecke, H.-P. Steinrück, K.H. Neyman, N. Rösch, Surf. Sci. 600 (2005) 78.

[8] H. Gabasch, S. Penner, B. Jenewein, B. Klötzer, A. Knop-Gericke, R. Schlögl, K. Hayek, J. Phys. Chem. B 110 (23) (2006) 11391.

[9] J.A. Rodriguez, Prog. Surf. Sci. 81 (2006) 141.

[10] Z. Chen, K.M. Neyman, N. Rösch, Surf. Sci. 548 (2004) 291.

[11] K.M. Neyman, R. Sahnoun, C. Inntam, S. Hengrasmee, N. Rösch, J. Phys. Chem. B 108 (2004) 5424.

[12] Z. Chen, K.M. Neyman, A.B. Gordienko, N. Rösch, Phys. Rev. B 68 (2003) 075417.

[13] K.M. Neyman, K.H. Lim, Z.-X. Chen, L.V. Moskaleva, A. Bayer, A. Reindl, D. Borgmann, R. Denecke, H.-P. Steinrück, N. Rösch, PCCP 9 (27) (2007) 3470.

[14] W. Stadlmayr, Ch. Rameshan, Ch. Weilach, H. Lorenz, M. Hävecker, R. Blume, T. Rocha, D. Teschner, A. Knop-Gericke, D. Zemlyanov, S. Penner, R. Schlögl, G. Rupprechter, B. Klötzer, N. Memmel, J. Phys. Chem. C 114 (2010) 10850.

[15] A.-P. Tsai, S. Kameoka, Y. Ishii, J. Phys. Soc. Jpn. 73 (2004) 3270.

[16] P. Bera, J.M. Vohs, J. Phys. Chem. C 111 (19) (2007) 7049.

[17] K.H. Lim, Z.X. Chen, K.M. Neyman, N. Rösch, J. Phys. Chem. B 110 (2006) 14890.

[18] K.H. Lim, L. Moskaleva, N. Rösch, ChemPhysChem 7 (2006) 1802.

[19] H. Lorenz, S. Turner, O.I. Lebedev, G. van Tendeloo, B. Klötzer, C. Rameshan, K. Pfaller, S. Penner, Appl. Catal. A 374 (2010) 180.

[20] H. Lorenz, M. Stöger-Pollach, S. Schwarz, K. Pfaller, B. Klötzer, S. Penner, Appl. Catal. A 347 (2008) 34.

[21] T. Bielz, H. Lorenz, W. Jochum, R. Kaindl, F. Klauser, B. Klötzer, S. Penner, J. Phys. Chem. C 114 (19) (2010) 9022.

[22] T. Bielz, H. Lorenz, P. Amann, B. Klötzer, S. Penner, J. Phys. Chem. C 115 (2011) 6622.

[23] T. Shido, Y. Iwasawa, J. Catal. 140 (1993) 575.

[24] A. Ueno, T. Onishi, K. Tamaru, Trans. Faraday Soc. 66 (1970) 756.

[25] W. Jochum, S. Penner, K. Föttinger, R. Kramer, G. Rupprechter, B. Klötzer, J. Catal. 256 (2008) 278.

[26] W. Reichl, G. Rosina, G. Rupprechter, C. Zimmermann, K. Hayek, Rev. Sci. Instr. 71 (3) (2000) 1495–1499.

[27] A. Knop, E. Kleimenov, M. Hävecker, Adv. Catal. 52 (2009) 213–272.

[28] a S. Tanuma, C.J. Powell, D.R. Penn, Surf. Interface Anal. 20 (1) (1993) 77–89;
b S. Tanuma, T. Shiratori, T. Kimura, K. Goto, S. Ichimura, C.J. Powell, Surf. Interface Anal. 37 (2005) 833–845.

[29] W. Stadlmayr, private communication.